Journal Pre-proofs

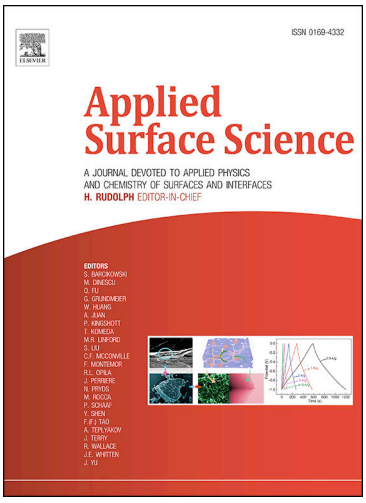

Full Length Article

Understanding the Interaction of Organic Corrosion Inhibitors with Copper at the Molecular Scale: Benzotriazole on Cu(110)

M. Turano, M. Walker, F. Grillo, C. Gattinoni, J. Edmondson, O. Adesida, G. Hunt, P. Kirkman, N.V. Richardson, C.J. Baddeley, A. Michaelides, G. Costantini

PII: S0169-4332(21)02261-3
DOI: https://doi.org/10.1016/j.apsusc.2021.151206
Reference: APSUSC 151206

To appear in: *Applied Surface Science*

Received Date: 13 July 2021
Revised Date: 3 September 2021
Accepted Date: 4 September 2021

Please cite this article as: M. Turano, M. Walker, F. Grillo, C. Gattinoni, J. Edmondson, O. Adesida, G. Hunt, P. Kirkman, N.V. Richardson, C.J. Baddeley, A. Michaelides, G. Costantini, Understanding the Interaction of Organic Corrosion Inhibitors with Copper at the Molecular Scale: Benzotriazole on Cu(110), *Applied Surface Science* (2021), doi: https://doi.org/10.1016/j.apsusc.2021.151206

Understanding the Interaction of Organic Corrosion Inhibitors with Copper at the Molecular Scale: Benzotriazole on Cu(110)

M. Turano[1], M. Walker[1], F. Grillo[2], C. Gattinoni[3,4], J. Edmondson[1], O. Adesida[1], G. Hunt[5], P. Kirkman[5], N. V. Richardson[2], C. J. Baddeley[2], A. Michaelides,[6] G. Costantini[1]

[1]Department of Chemistry, University of Warwick, Coventry, CV4 7AL, UK.
[2] EaStCHEM-School of Chemistry, University of St. Andrews, St. Andrews, KY16 9ST, UK.
[3]Department of Materials, ETH Zurich, CH-8093 Zürich, Switzerland.
[4]School of Engineering, London South Bank University, London, SE1 0AA, UK.
[5]Strategic Research, Lubrizol Limited, Nether Lane, Hazelwood, DE56 4AN, UK.
[6]Yusuf Hamied Department of Chemistry, University of Cambridge, Cambridge, CB2 1EW, UK.

Abstract

Benzotriazole (BTAH) has been used for several industrial applications, but most commonly as a corrosion inhibitor for copper, since the 1950s. However, the mechanism of its interaction with copper surfaces at the atomistic scale is still a matter of debate. Here, the adsorption of BTAH onto a clean Cu(110) surface has been investigated by a combination of scanning tunnelling microscopy, X-ray photoelectron spectroscopy, high resolution electron energy loss spectroscopy and density functional theory calculations. Different supramolecular structures have been observed depending on molecular coverage and annealing. In the low coverage regime, flat lying deprotonated species are formed which give way to benzotriazolate molecules in an upright configuration by increasing the BTAH exposure. The ensuing monolayer is self-limiting but, upon annealing above 150 °C, transforms into a highly ordered nano-ridge structure resulting from a significant in-plane and out-of-plane reconstruction of the surface. All structures are characterised by a strong molecule-substrate interaction and the high coverage phases are dominated by the formation of metal-organic complexes between copper adatoms and benzotriazolate species. These findings shed light on the nature and strength of the interaction occurring between BTAH and copper which lies at the basis of the effectiveness of this prototypical corrosion inhibitor.

1. Introduction

The corrosion of metals and its prevention play a very important role in industry due to its high economic impact[1]. Indeed, recent studies estimated the annual global cost of corrosion to be US$2.5 trillion[2]. Copper is a material of great interest in this context, as it is widely used in many areas such as metallurgical industries, electrical power and electronics industries, automotive manufacturing and telecommunications[3]. The main reason behind its versatility is the combination of excellent electrical and thermal conductivities, although the relative ease by which copper can undergo tarnishing and corrosion often represents a challenge to its applications[4],[5]. As a result, protection of copper and its alloys is a topic of particular interest that has attracted a great deal of research efforts over the years. One way to achieve this is through the use of organic corrosion inhibitors which form self-assembled monolayers (SAMs). These SAMs are typically ultrathin organic films where chemisorbed molecules spontaneously organise into a self-limiting single layer with high molecular order and density that can act as a physical and chemical barrier against corrosion and dissolution[6]. Throughout the years, much attention has been given to benzotriazole (BTAH, Fig. 1a) and its derivatives as a class of multifunctional corrosion inhibitors due to their ability to protect copper and its alloys under various media[7]. BTAH has been widely used in industry since the 1950s[8] and it is known that it forms an insoluble, strong and two-dimensional barrier film against several oxidising agents[9]. However, its molecular adsorption, orientation and chemical state on copper surfaces have been debated for many years[10-12] and the precise mechanism of its action is still not known[1]. There have been propositions that the effectiveness of BTAH depends on its ability to chemisorb and form Cu(I)–BTA complexes[13] but a clear and fully evidence-supported atomic and molecular scale picture is still missing. Indeed, apparently contradictory data can be found in the literature for the molecular adsorption and orientation of BTAH on copper, which in different studies was reported as upright, inclined or flat with respect to the metal surface[1, 12, 14, 15].

In an attempt to answer these questions, it is desirable to start with simple model systems in order to attain a deeper understanding based on strong experimental and theoretical evidence. This can be achieved by studying the interaction of BTAH in ultra-high vacuum (UHV) conditions with atomically flat and clean single crystal substrates, starting from the three main low Miller indices copper surfaces. The most reliable studies so far have been conducted on the Cu(111) orientation, where it has been shown that BTAH is able to form several different and complex structures[16-19].

These studies suggested that upright, chemisorbed species commonly form by deprotonation of BTAH to benzotriazolate, BTA, and coordination with free copper adatoms or low coordinated copper atoms such as at step edges and surface defects. It has been suggested that these features are likely to be in the form of $Cu(BTA)_2$ and Cu(BTA) complexes in the low coverage regime. At higher surface coverage, scanning tunnelling microscopy (STM) data revealed a pseudohexagonal pattern formed by these complexes, which was also observed in the full monolayer regime and showed good agreement with density functional theory (DFT) calculations on the same system. Much less information is available for the interaction of BTAH with the other two, low Miller index surfaces, with a single STM and low electron energy diffraction (LEED) study performed on Cu(110) reporting the formation of a flat lying BTA phase with a c(4×2) unit cell[20]. Conversely, on Cu(100) a study, using near edge X-ray absorption fine structure (NEXAFS) spectroscopy, suggested that deprotonated BTA molecules re-oriented from an almost upright to a more flat configuration by increasing the coverage from monolayer to multilayer[15].

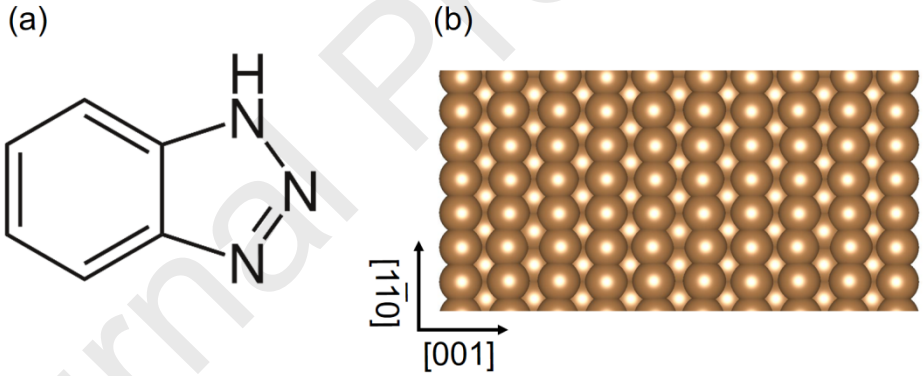

Fig. 1. Corrosion inhibitor molecule and cupper substrate used in this study. (a) Structure of the BTAH molecule. BTA, the deprotonated form of BTAH, is obtained by removing the triazole hydrogen. (b) Atomic structure of the Cu(110) surface; the two principal crystallographic directions $[1\bar{1}0]$ and $[001]$, respectively, are explicitly indicated.

2. Material and methods

Cu(110) single crystal surfaces were prepared by a series of Ar^+ ion sputtering cycles (4 μA/cm^2 for 15 minutes) followed by annealing (500 °C, 10 minutes). BTAH has a relatively high vapour pressure at room temperature, which prevents its storage in UHV and complicates its transfer to surfaces by molecular beam deposition. As a consequence, BTAH was stored as a solid powder in a glass crucible separated from the UHV preparation chamber through an angle valve. Prior to deposition, the

crucible was pumped for a few hours by means of a 300 l/s turbomolecular pump backed by a scroll pump. In order to achieve better control over the molecular pressure, the crucible was cooled by immersing it into a mixture of ice and sodium chloride until a stable temperature of about −10 °C was reached. Molecular deposition was then performed by opening the valve to the preparation chamber and backfilling it with a BTAH pressure in the range of 10^{-8}–10^{-7} mbar, measured with an ion gauge. The base pressure of the preparation chamber was 1×10^{-9} mbar. Different molecular exposures were obtained by varying the time the valve was kept open. It should be noted that the values of BTAH exposure, typically expressed in langmuir, might vary from one UHV system to another, mostly due to variations in the pressure reading (calibration and position of the pressure gauges).

STM measurements were carried out by transferring the samples to a neighbouring UHV chamber separated by a gate valve, that hosts a commercial variable temperature STM. Samples were typically cooled to around −140 °C before being imaged, in order to decrease molecular surface diffusion. This improved the image quality – with respect to room temperature measurements – for the lowest density phases. However, the compact molecular phases showed no change between room temperature and low temperature imaging, demonstrating their thermal stability in this range. The STM was operated in constant current mode and the tunnelling current, I, and bias voltage, V_{bias} (applied to the sample), are explicitly indicated for each of the presented images. The WSXM software package was used to process the STM data[21].

X-ray photoelectron spectroscopy (XPS) measurements were performed in a separate UHV system that also included a LEED setup. The Cu(110) single crystal was prepared similarly to that for the STM experiments and its order and cleanliness were checked by LEED and XPS prior to molecular deposition. The same technique used for transferring BTAH to the Cu(110) surface in the STM experiments was used here. XPS measurements were performed using a monochromatic Al Kα X-ray source (photon energy of 1486 eV). The CasaXPS software[22] was used for analysing XPS data. The procedure for fitting the XP spectra is described in detail in the supplementary material (SM).

High-resolution electron energy loss spectroscopy (HREELS) measurements were carried out in a separate UHV system, where the substrate and the molecular films were prepared similarly to those for the STM and XPS experiments. The spectrometer was operated in the specular geometry ($\vartheta_i = \vartheta_f = 45°$) with a nominal primary beam energy of 8 eV and a typical elastic peak resolution of *ca.* 50 cm^{-1} (6.2 meV full width at half maximum, FWHM). Spectra were normalised to the intensity

of the elastic peak. For comparison with HREEL spectra, gas phase DFT calculations of several Cu_xBTA_y species were performed using the B3LYP functional and the 6-311G basis set as implemented in Gaussian09[23]. Vibrational spectra were calculated after geometrical optimisation. Energy scales were corrected according to the formula proposed by Kasahara and co-workers[24] to compensate for the overestimation due to the functional/basis set combination. Calculated peaks were convoluted with Gaussian functions having FWHM of 50 cm^{-1}. To simulate the decrease in sensitivity at increased energy loss typical of HREELS, empirically, each intensity was divided by its respective frequency.

Simulations of BTAH adsorbed on Cu(110) have been performed with the VASP[25-27] code with the optB86b-vdW functional[28]and the projector augmented wave (PAW) method[29]. The kinetic energy cut-off on the planewave basis set was 400 eV. The Monkhorst-Pack k-mesh used for the bulk copper unit cell is 13×13×13 *k*-points and the optimisation was run until the forces on the ions were lower than 5×10^{-4} eV/Å. With these parameters the lattice constant of copper is a_{DFT} = 3.606 Å, matching perfectly the experimentally reported value a_{exp}=3.61 Å[30]. We also obtained very good agreement between calculated and experimental bond length on benzotriazole, as reported in the SM. Four-layer-thick Cu(110) slabs were used, with a range of surface unit cells, having surface areas of 3×5, 3×8, 1×8, 4×2 with respect to the Cu(110) (1×1) unit cell. The Monkhorst-Pack *k*-point meshes for such systems are (3,3,1), (3,2,1), (3,2,1), (3,2,1), respectively. In all unit cells *ca.* 20 Å of vacuum was placed between the copper slabs in the surface normal direction and the ionic coordinates of the bottom copper layer were kept fixed at bulk values. Convergence of all the settings was thoroughly checked[18]. The adsorption energies, E_{ads}, were calculated as:

$$E_{ads} = E_{system} - N_{BTA}E_{BTA} - E_{slab} + N_{Cu}E_{Cu}^{form} \quad (1)$$

where E_{system} is the total energy of the whole system, consisting of deprotonated BTAH molecules (i.e. BTA radicals) adsorbed on the copper slab. E_{BTA} and E_{slab} are, respectively, the total energies of the BTA radical in the gas phase and of the fully relaxed Cu(110) substrate. The substrate might include copper adatoms, whose formation energy, E_{form}^{Cu}, is calculated as the energy needed to add a bulk atom onto a clean surface and it amounts to $E_{Cu}^{form} =$ 0.35 eV for Cu(110). N_{BTA} and N_{Cu} are the numbers of BTA and copper adatom species considered, respectively.

3. Results and Discussion

The results are organised in terms of experimental and theoretical techniques used to obtain the data (STM, DFT, XPS and HREELS) and presented following an increasing exposure of the Cu(110) to the BTAH vapour.

3.1. Scanning Tunnelling Microscopy

3.1.1. Low coverage regime

A freshly cleaned Cu(110) surface was exposed to a BTAH pressure of 1.3×10^{-8} mbar for 60 seconds, corresponding to 0.6 langmuir. Larger area STM images (Fig. 2a) show the formation of an extended molecular layer that covers the entire surface. Significantly reconstructed Cu(110) monoatomic step edges are clearly recognisable running along the $[\bar{1}11]$ and $[1\bar{1}1]$ surface directions and are a first indication of a strong interaction between BTAH and the copper substrate. XPS measurements (*vide infra*) show that the molecules deprotonate upon adsorption and that the species present on Cu(110) are actually benzotriazolates (BTA), in agreement with previous results in the literature[20]. Higher resolved STM images (Figs. 2b,c) show the presence of locally ordered structures composed of bright dots, whose size is compatible with that of individual flat-lying BTA species. Two main structures, a lower and a higher density phase, can be observed. At very low molecular coverage, the lower density phase is predominant (see Fig. S1) but, by increasing the exposure time to the BTAH vapour pressure, most of the surface is characterised by the higher density phase coexisting with only small patches of the low density one (e.g. central lower part of Fig. 2b).

The lower density phase is characterised by regions that are relatively closed-packed but disordered, coexisting with ordered regions whose lateral extension appears to increase with increasing molecular coverage. These latter regions have a close-to-square symmetry, with a unit cell oriented parallel to the two main surface directions $[1\bar{1}0]$ and $[001]$. The molecular periodicity along $[1\bar{1}0]$ is ~0.77 nm, compatible with a $\times3$ unit spacing with respect to the Cu(110) atomic lattice in this direction. Along $[001]$ the molecular periodicity is ~0.76 nm, which is compatible with a $\times2$ unit spacing with respect to Cu(110) substrate. Overall, based on the STM data, this phase is therefore locally organised into a commensurate (3×2) superlattice with a theoretical molecular density of 1.8 molecules/nm^2, while the density measured from the STM images is (1.6 ± 0.2) molecules/nm^2. We

note that the limited resolution of the STM images does not allow us to distinguish the molecular orientation within this phase.

The higher density phase (upper part of Fig. 2b and whole of Fig. 2c) is characterised by rows of molecules directed along $[001]$ with a periodicity of (0.78 ± 0.08) nm, compatible with a ×2 unit spacing with respect to this orientation of the Cu(110) surface. The rows are separated by (0.55 ± 0.05) nm in the $[1\bar{1}0]$ direction, compatible with a ×2 unit spacing with respect to the Cu(110) atomic lattice. However, neighbouring rows are offset with respect to each other by one substrate unit spacing along $[001]$. Thus, the analysis based on the STM data indicates the presence of a c(4×2) commensurate structure. The expected molecular density for a c(4x2) superstructure is 2.7 molecules/nm^2, while the density determined directly from the STM images is (2.1 ± 0.2) molecules/nm^2.

For certain tip conditions, it is possible to achieve some sub-molecular contrast in the c(4×2) structure by distinguishing two sub-units, one larger than the other. These are tentatively assigned to the benzene and triazole rings, respectively, on grounds of size and electronic configuration. Based on this, the orientation of the BTA molecules within the unit cell can be proposed, resulting in the best estimate for the adsorption model shown in Fig. 2d, where we are assuming that the molecules are essentially flat and pointing toward the $[\bar{1}1\bar{1}]$ direction. This model shows that, if the molecules were indeed completely flat, they would be extremely close to each other, resulting in unrealistic steric hindrances. This gives us a first indication that the molecules cannot be completely flat, something that is further supported by the HREELS measurements and by the DFT calculations (*vide infra*). This model also implies the existence of four equivalent domains obtained by rotations of 180° and reflections with respect to principal substrate crystallographic directions (Fig. S2). It should be further noted that from our STM (and XPS, *vide infra*) measurements we cannot determine whether adatoms are included within the observed supramolecular structures. Theoretical studies have shown that adatoms generally stabilise the interaction of BTAH with copper, as they allow a larger number of strong Cu−N bonds to be formed[18, 31, 32]. Moreover, the formation of metal-organic complexes with substrate adatoms has been proposed for several other organic molecules that become anions upon adsorption on metallic substrates, such as, for example, various benzene carboxylic acids[33-36], ketone[37, 38], pyrimidine[39] or cyano-containing electron acceptors[40-42]. For the latter in particular, the presence of adatoms has been directly proven through a combination of experimental quantitative structure determination and

DFT calculations[43]. However, the DFT calculations show that for the c(4×2) phase of BTA on Cu(110) the presence of adatoms is not favourable (*vide infra*).

Figure 2b shows that the c(4×2) structure is highly defective, with ordered domains extending only for an average of (2.3 ± 0.2) nm in the $[001]$ direction and for (1.7 ± 0.2) nm in the $[\bar{1}1\bar{1}]$ direction and the domains being separated by darker lines that run along $[001]$, $[\bar{1}11]$ and $[\bar{1}1\bar{1}]$. The nature of these domain boundaries can be determined by superposing a carefully scaled molecular model of the c(4×2) superstructure onto high resolution STM images. For example, with reference to Fig. 2c, it is possible to establish that two neighbouring, ordered translational domains, separated by a $[\bar{1}11]$-oriented darker line are shifted with respect to each other by ~1 nm along the [001] direction which is compatible with a separation of ×3 substrate units. Therefore, the darker lines are most probably very small regions of exposed copper substrate that separate small c(4×2) domains along the $[001]$, $[\bar{1}11]$ and $[\bar{1}1\bar{1}]$ surface directions (see model in Fig. S3). Effectively, these can be thought as dislocations within the c(4×2) molecular superstructure and are most probably caused by the competition between molecule-molecule and molecule-surface interactions, as has been suggested for other molecular systems[44, 45]. In Fig. 2 it is also possible to distinguish quite clearly a few parallel straight lines composed of pairs of brighter dots with an apparent height of ~1.8 Å with respect to the first molecular layer. These double-dot chains separate different c(4×2) domains and run along the same $[\bar{1}11]$ and $[1\bar{1}1]$ surface directions that delimit the reconstructed surface steps. While their origin is still unclear, this observation could suggest that the chains are composed of pairs of BTA molecules coordinated to copper adatoms. Overall, our description of the low coverage regime of BTAH on Cu(110) is in agreement with previous data [20, 46, 47] although earlier papers only reported the molecular periodicity of the c(4×2) phase.

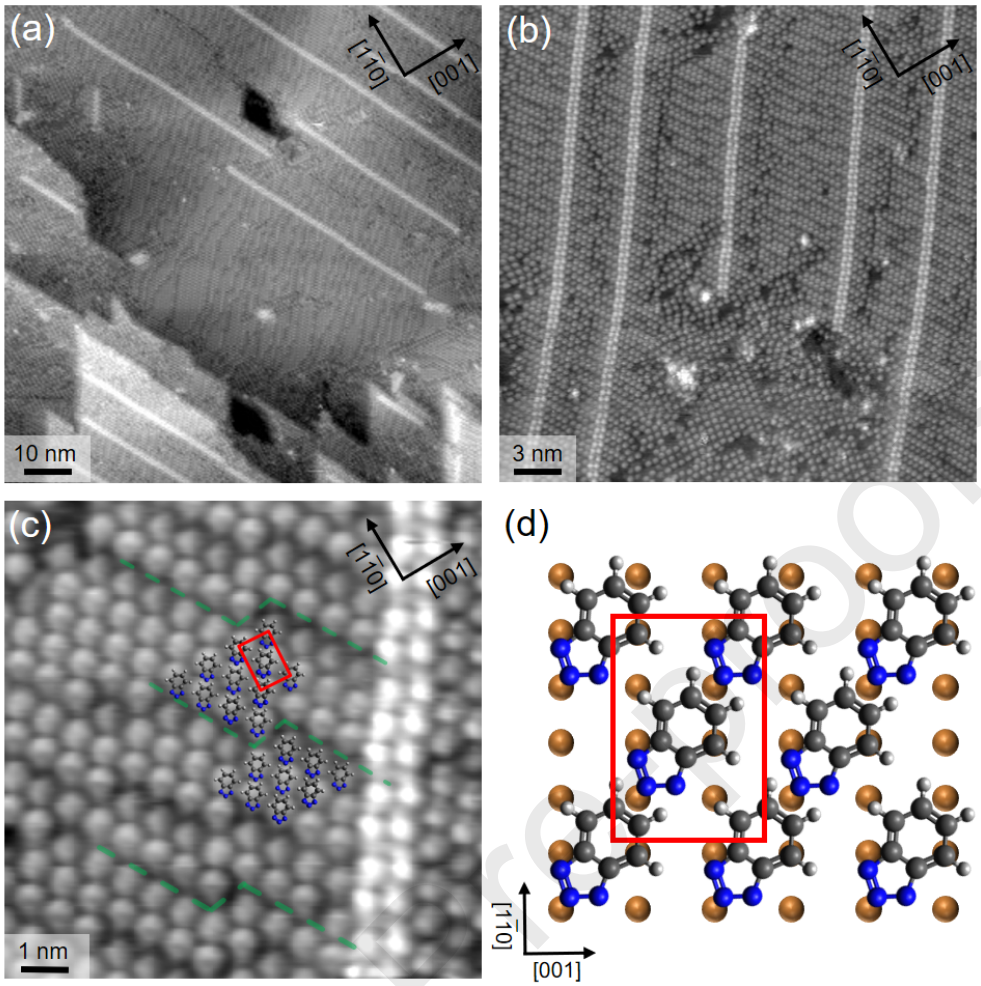

Fig. 2. Low coverage regime of BTA on Cu(110). (a) Large area STM image (88 × 88 nm^2) showing significantly reconstructed step edges. (b) 30 x 30 nm^2 image showing the coexistence of the c(4×2) with the lower density (3×2) phase (the latter is visible in the bottom-centre part of the image). (c) High resolution image of the c(4×2) phase with superimposed molecular model. The red rectangle shows the unit cell of the supramolecular structure, while green dashed lines indicate dislocations between small ordered regions. (d) Molecular model proposed for the c(4×2) superstructure. The model assumes a fully flat adsorption geometry resulting in unrealistic steric clashes (see main text). For clarity, only the copper atoms in the topmost copper layer are shown, i.e. the close-packed $[1\bar{1}0]$ rows. Tunnelling parameters were I = 60 pA, V_{bias} = –0.6 V in (a), I = 100 pA, V_{bias} = –0.6 V in (b) and I = 100pA, V_{bias} = –0.6 V in (c).

3.1.2. High coverage regime

Increasing the exposure of the Cu(110) surface to the BTAH gas up to *ca*. 1.4 langmuir, results in the appearance of a new phase. Initially, by adding a small amount of extra BTAH, this new phase coexists with the c(4×2) and develops in thin stripes – mostly oriented along the $[001]$, $[\bar{1}11]$ and $[1\bar{1}1]$ surface directions – that appear in between ordered c(4×2) domains (Fig. S4a). By comparing

the position and the relative registries of the molecules in adjacent c(4×2) domains, it is possible to conclude that the new phase nucleates at dislocations and domain boundaries in the c(4×2) structure (see Fig. S4b).

Further increases in BTAH exposure cause the extension of the regions covered by the new phase until this occupies the entire surface (Fig. 3a). Reconstructed surface step edges can be recognised running along $[\bar{1}11]$ and $[1\bar{1}1]$ (Fig. 3b), the same as those observed in Fig. 2a for the lower density phase. Higher resolution STM images allow individual elongated bright dots within the molecular layer to be distinguished (Figs. 3b and 3c), whose lateral dimensions and separation are too small to be compatible with flat-lying BTA molecules. A better fit is obtained with molecules in an upright (or close to upright) configuration (Fig. 3c) with their molecular plane aligned along the $[1\bar{1}0]$ direction. This indicates that a transition from a mostly flat to a mostly upright configuration is occurring by increasing the molecular coverage, an interpretation which is confirmed by the HREELS measurements (*vide infra*). The elongated dots appear to be generally aligned parallel to each other and arranged into wavy rows composed of short straight segments (Fig. 3c); the latter are mainly oriented along three surface directions: $[001]$, $[1\bar{1}4]$ and $[1\bar{1}2]$ (and along those equivalent by reflection and rotation symmetry). The molecular periodicity along the $[001]$ rows is (0.37 ± 0.04) nm, i.e. compatible with a ×1 periodicity with respect to the Cu(110) substrate, along the same direction. This intermolecular separation is consistent with the parallel π-π stacking distance between aromatic rings[48, 49], representing a further indication that the molecules are adsorbed in an upright fashion. The minimum separation between molecules along $[1\bar{1}0]$ (i.e. perpendicular to the $[001]$-rows) is of (0.76 ± 0.08) nm, consistent with ×3 substrate periodicity in this direction. Thus, in this high coverage phase, the BTA molecules appear to be organised into a (3×1) local arrangement with respect to the underlying Cu(110) surface. The expected molecular density for a (3×1) superstructure is 3.6 molecules/nm^2, while the density measured from the STM images is (3.5 ± 0.3) molecules/nm^2.

The other two main directions of the molecular rows can be rationalised by considering that, besides the parallel (or sandwich) configuration, the π-π stacking between successive BTA molecules could also be of the parallel-displaced type[38]. Molecular rows oriented along $[1\bar{1}2]$ form an angle of 34° ± 3° with respect to $[001]$ and two neighbouring molecules are separated by (0.39 ± 0.06) nm. This is compatible with successive molecules within a row being shifted with respect to each other by one substrate unit lattice along both $[001]$ and $[1\bar{1}0]$ (see model highlighted by the green line in

Fig. 3d, expected angle with $[001]$ of ~35°), and thus interacting through parallel-displaced π-π stacking (average distance from the literature ~0.38 nm[50]). Similarly, molecular rows along $[1\bar{1}4]$ form an angle of ~19° with $[001]$ and are compatible with a regular alternation of a parallel and parallel-displaced π-π stackings (see model highlighted by the cyan line in Fig. 3d, expected angle with $[001]$ of ~20°).

Often the elongated bright dots tend to form local pairs along the $[1\bar{1}0]$ direction, leaving a larger separation to the following pair (see Fig. S5a). Although in this phase this organisation does not extend into a long-range ordered pattern, it is partially responsible for the wavy appearance of the molecular rows. Most probably these local pairs are a first manifestation of the $Cu(BTA)_2$ complexes that dominate the surface morphology after annealing (*vide infra*) and that have been reported for the BTA/Cu(111) system[16-18]. Also here, the STM measurements cannot establish the presence (or absence) of adatoms within the molecular rows. However, DFT calculations give a clear indication for a significant energy gain achieved by binding two upright BTA molecules with one copper adatom into a $[1\bar{1}0]$-oriented $Cu(BTA)_2$ metal-organic complex (*vide infra*). The energetically most favourable phase at high molecular coverage should thus be characterised by $[001]$-oriented double chains formed by the periodic succession of $Cu(BTA)_2$ complexes in a (6×1) superstructure (see DFT section). The fact that experimentally this is only observed locally and that Cu(BTA) complexes appear to be more frequent than $Cu(BTA)_2$ species (see HREELS section), is probably the result of kinetic limitations during the growth of the molecular layer.

The high coverage phase is essentially self-limiting since by increasing the exposure of BTAH up to ≈6 langmuir, no major changes were observed in the STM images. This is compatible with what is measured by XPS (*vide infra*). However, the occasional presence of small 'fuzzy' areas was sometimes observed (e.g., top right of Fig. 3b). Most likely, they represent patches of a physisorbed second layer of molecules that are highly mobile and thus not well resolved by STM.

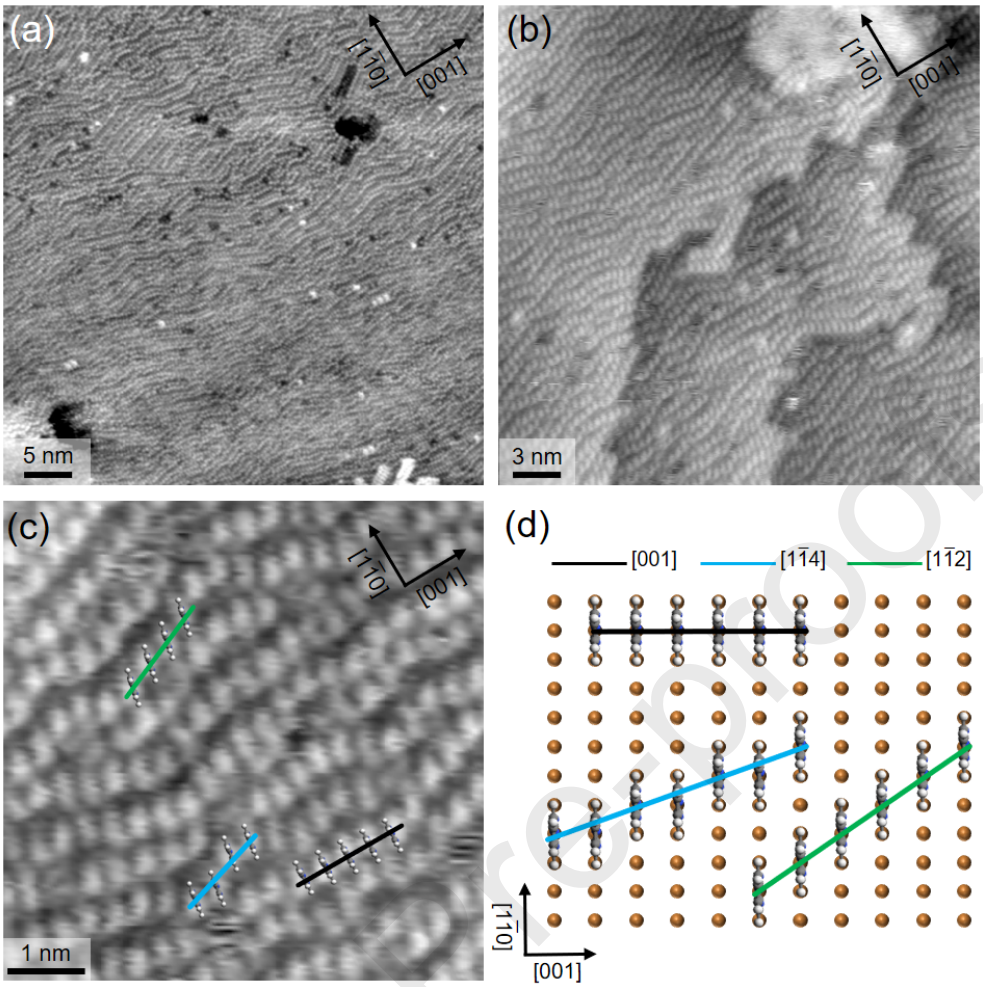

Fig. 3. High coverage regime of BTA on Cu(110). (a) Large area STM image (50 x 50 nm^2). (b) 30 x 30 nm^2 image showing that the surface is covered by wavy molecular rows with short straight segments. Clearly reconstructed step edges are also visible. (c) High resolution image with superimposed models of upright BTA molecules, demonstrating the three main directions of the molecular rows: $[001]$, $[1\bar{1}2]$ and $[1\bar{1}4]$ identified by black, green and cyan lines respectively. (d) Corresponding molecular models on the Cu(110) surface. For clarity, only the copper atoms in the topmost copper layer are shown. Tunnelling parameters were I = 100 pA, V_{bias} = –1.0 V in (a), I = 100 pA, V_{bias} = –0.6 V in (b) and I = 100pA, V_{bias} = –1.0 V in (c).

3.1.3. 3D nano-ridges

Figures 4a and 4b show that annealing the high coverage phase to 150 °C results in a major transformation of the surface morphology which appears to be dominated by 3D nano-ridges selectively oriented along two directions, $[1\bar{1}\bar{2}]$ and $[1\bar{1}2]$, that are mirror-symmetric with respect to the principal surface orientations of Cu(110). Higher resolution STM images reveal the presence of extremely regular parallel rows of features elongated in the $[3\bar{3}2]$ direction and aligned with the

3D nano-ridges (e.g. Fig. 4c). The shape and size of these dots is very similar to those in Figure 3, and in fact they are compatible with essentially upright molecules (see superposed molecular model in Fig. 4c). Their periodicity along $[1\bar{1}\bar{2}]$ is (0.46 ± 0.04) nm, compatible with the expected distance between successive equivalent Cu(110) surface sites in this direction (~0.44 nm). In a few cases (e.g. central row in Fig. S6a), a single $[1\bar{1}\bar{2}]$–oriented molecular row terminates the peak of a nano-ridge. However, the top of most nano-ridges is constituted by two parallel rows of molecules at the same height, with successive neighbouring parallel rows being at increasingly lower heights. In particular, the measured height difference between neighbouring parallel rows is ~1.3 Å, which is compatible with the height of a Cu(110) monoatomic step (~1.28 Å, see Fig. S6b).

All these observations lead to a proposed model for the nano-ridges being formed by a succession of narrow Cu(110) terraces, delimited by monoatomic step edges along $[1\bar{1}\bar{2}]$ and decorated by BTA molecules in an almost upright configuration. Most likely, molecules preferentially adsorb at the step edges, which represent the most reactive sites for the coordination of BTA and the formation of Cu_xBTA_y metal-organic complexes. The terraces have an average width of (4.9 ± 0.4) nm, which corresponds to a typical extension of about 20 atoms along $[1\bar{1}0]$. When a nano-ridge is terminated with a double molecular row (e.g. in Fig. 4c), neighbouring molecules on the apex of the ridge are most probably bonded to a single adatom located between them, forming $Cu(BTA)_2$ metal-organic complexes which are similar to those observed for the deposition of BTA on Cu(111)[16, 19] and are shown to be energetically favourable by DFT calculations (*vide infra*). A schematic of this model is shown in Fig. 4d. The complexes are expected to interact with each other through π-π stacking of the aromatic rings of successive BTA molecules along $[1\bar{1}\bar{2}]$. Assuming that each of the elongated dots in the high-resolution STM images corresponds to an individual molecule, the measured molecular density for the 3D nano-ridges phase is 3.2 ± 0.3 molecules/nm^2, which is very similar to the density measured before annealing.

This radical change in the surface morphology implies a strong in-plane and vertical reconstruction of the Cu(110) substrate and can only be rationalised through a considerable transport of copper atoms both parallel and perpendicular to the surface, promoted by the presence of BTA and by its strong interaction with copper atoms. Annealing the sample up to 250 °C does not result in any observable change. At 300 °C the surface becomes quite rough and, despite this limiting the resolution that can be attained in the STM images, there seems not to be any presence of the molecules, indicating a possible thermal desorption of BTA[17].

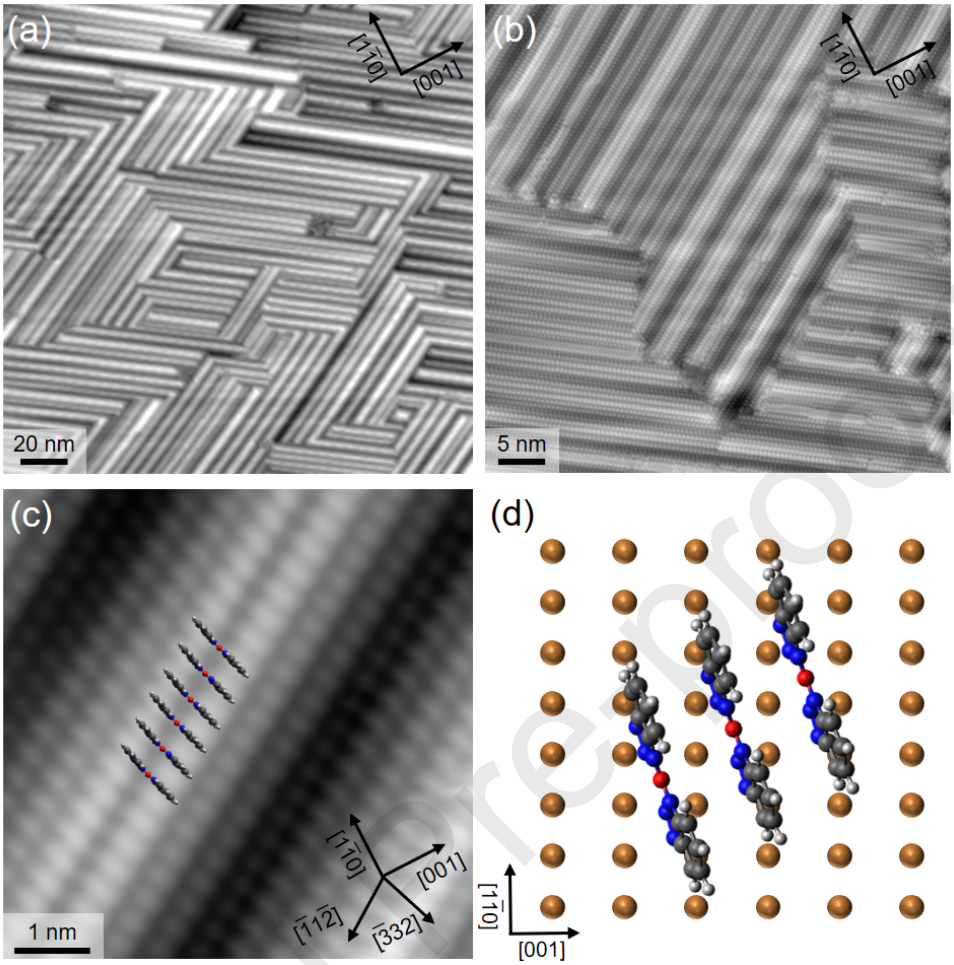

Fig. 4. 3D nano-ridges induced by annealing the high coverage phase of BTA on Cu(110). (a) Large area STM image (140 x 140 nm^2) showing that the nano-ridges are oriented along two preferential surface directions. (b) 50 x 50 nm^2 image showing that the nano-ridges are decorated by a highly regular arrangement of upright BTA molecules. (c) High resolution image displaying the details of a single nano-ridge. A few scaled models of the $Cu(BTA)_2$ metal-organic complexes are superposed onto the image. (d) Corresponding molecular model on the Cu(110) surface. The red spheres, represent copper adatoms coordinated to pairs of BTA molecules and are tentatively positioned in hollow sites of the substrate that are consecutive along $[1\bar{1}\bar{2}]$. For clarity, the Cu(110) substrate is shown in its unreconstructed form and only the atoms in the topmost layer are displayed. Copper adatoms are red. Tunnelling parameters were I = 100 pA, V_{bias} = −1.0 V in (a), I = 100 pA, V_{bias} = −1.0 V in (b) and I = 100 pA, V_{bias} = −1 V in (c).

3.2. Density Functional Theory

3.2.1. Low coverage regime

With a view to aiding the interpretation of the STM and the other experimental measurements, we performed a series of DFT calculations for BTA on Cu(110), with and without copper adatoms. The three most stable structures found are shown in Fig. 5. The c(4×2) arrangement (Fig. 5a), is the overall most stable one, with an adsorption energy of $E_{ads} = -4.66$ eV per molecule. Low coverage $Cu(BTA)_2$ complexes arranged along the $[001]$ direction, shown in Fig. 5b, present flat-lying molecules and their adsorption energy is $E_{ads} = -4.0$ eV per molecule, i.e. 0.66 eV per molecule less stable than for the c(4×2) structure. A third low-energy structure is shown in Fig. 5c, and it includes a BTA molecule with a copper adatom. This structure has an adsorption energy $E_{ads} = -3.87$ eV per molecule, i.e. 0.69 eV per molecule less stable than the c(4×2). It is worth noting that the adatom formation energy does not affect the energy ordering between the three structures. Indeed, even without including it in Eq. 1 (that is, by removing the last term of Eq. 1) the c(4×2) structure shown in Fig. 5a is more energetically stable than the structures in Figs. 5b and 5c by 0.32 eV per molecule and 0.45 eV per molecule, respectively.

The structure of the Cu(110) surface provides a good template for the adsorption of BTA molecules in the c(4×2) superstructure, without the need for additional adatoms. The adsorption is stabilised by the formation of three strong bonds between the azole moiety and surface Cu atoms, with a bond length of 2.0 Å in all three instances. Steric interactions between neighbouring BTAs are minimised by two mechanisms: the tilting of the molecular plane with respect to the surface by 21° and by a ~5° rotation along the c2 molecular axis. The tilt of the molecular plane is also suggested from the HREELS and STM results. The addition of an adatom in the formation of $Cu(BTA)_2$ or Cu(BTA) complexes, breaks this arrangement of Cu surface bonds and leads to the less stable structures shown in Figs. 5a and 5c, respectively, in stark contrast with the behaviour observed on Cu(111)[11, 18].

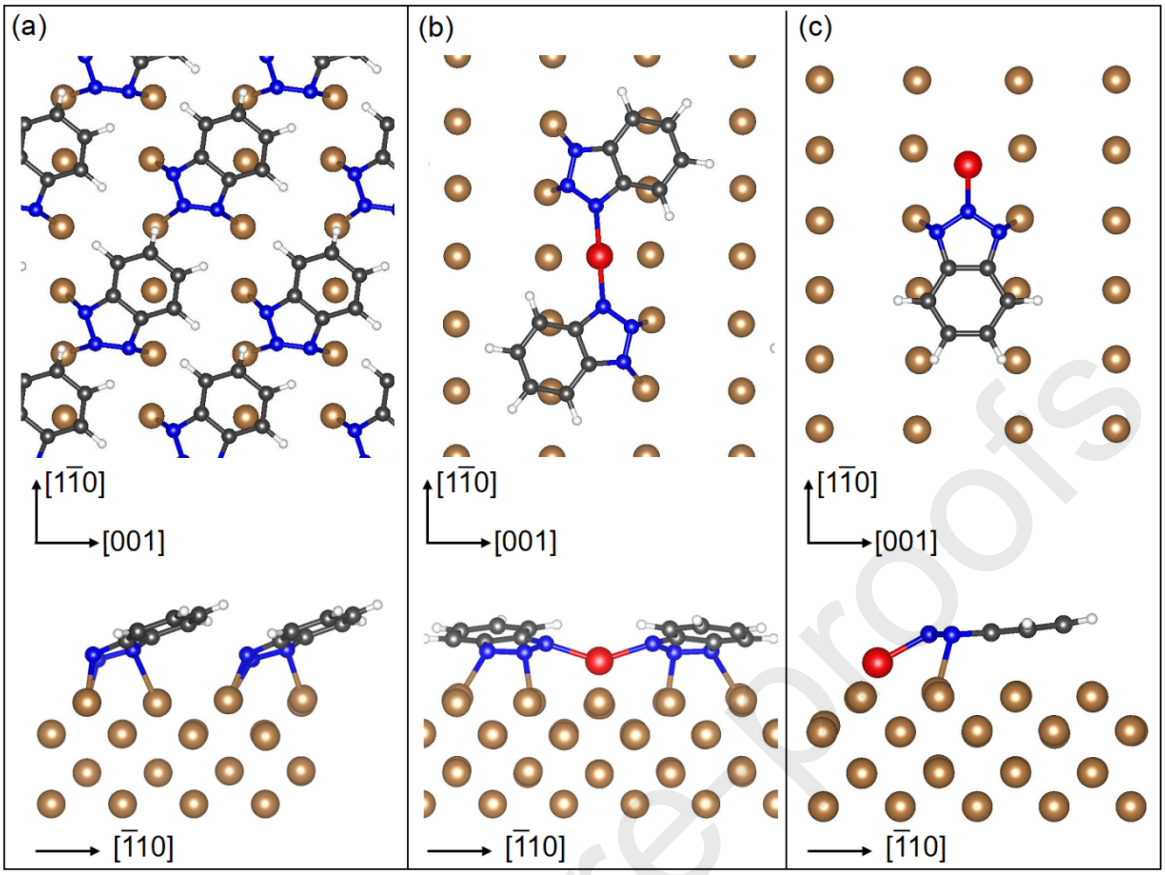

Fig. 5. DFT evaluated low-energy configurations of the low coverage phases of BTA on Cu(110). Top-view (upper row) and side-view (lower row) along the $[001]$ direction of (a) the periodic c(4×2) BTA superstructure, (b) low coverage $Cu(BTA)_2$ complex and (c) a BTA single molecule with a copper adatom. H atoms are white, C grey, N blue; the copper substrate atoms are brown and the copper adatoms are red.

3.2.2. High coverage regime

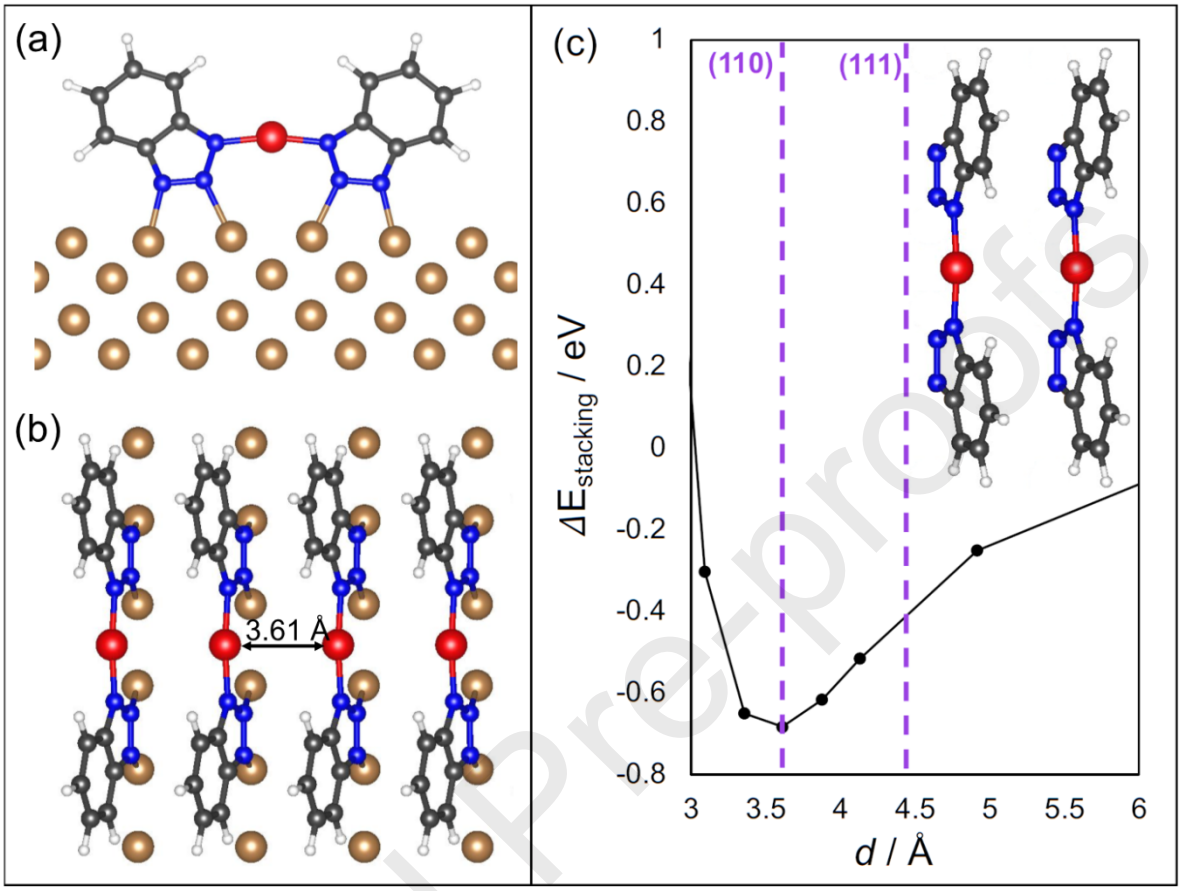

Fig. 6. DFT calculations of the high coverage phase of BTA on Cu(110). (a) Side view along the [001] direction and (b) top view of the lowest energy configuration of $Cu(BTA)_2$ metal-organic complexes on Cu(110) stacked in a (6×1) superstructure. For clarity, only the top-most layer of copper atoms is shown. (c) Plot of the energy of two gas-phase $Cu(BTA)_2$ complexes as a function of their separation *d*. The closest commensurate distances on Cu(110) and Cu(111) are indicated by vertical dashed lines. H atoms are white, C grey, N blue; the copper substrate atoms are brown and the copper adatoms are red.

At high coverage, STM images suggest the formation of upright BTA molecules organised in a local (3×1) or (6×1) arrangement. Our calculations show that $Cu(BTA)_2$ complexes composed of two upright molecules connected by a copper adatom (as shown in Fig. 6a and 6b) are the lowest-energy high-coverage structures and possess a (6×1) periodicity with respect to the Cu(110) substrate.

The dominance of the $Cu(BTA)_2$ complexes on the Cu(110) surface at high coverage is related to the synergy between their structure and that of the surface. Fig. 6b displays the lowest energy

configuration of Cu(BTA)$_2$ complexes on Cu(110), which is stabilised by the π-stacking interaction between the aromatic parts of the BTA molecules. Fig. 6c shows how the stacking energy, $E_{stacking}$, between two isolated Cu(BTA)$_2$ complexes varies with their distance d perpendicular to the molecular plane and it is calculated as: $E_{stacking} = E_{total}^{stacked} - 2 \times E_{total}^{Cu(BTA)_2}$, where $E_{total}^{stacked}$ is the DFT total energy of the system of two Cu(BTA)$_2$ complexes in the gas phase at a distance d, and $E_{total}^{Cu(BTA)_2}$ is the DFT total energy of a single Cu(BTA)$_2$ complexe in the gas phase. The graph is characterised by a clear minimum for $d = 3.65$ Å and has a relatively sharp increase for smaller and larger values. This optimal distance is very close (~1% larger) to 3.61 Å, which is the substrate lattice parameter of the Cu(110) substrate along $[001]$. Thus, the development of $[001]$-oriented double chains of BTA molecules formed by the periodic succession of Cu(BTA)$_2$ complexes in a (6×1) superstructure is energetically stable. As a matter of fact, this rather unique molecular structure is stabilised by two hierarchical successive levels of interactions. First there is the favourable orientation within each Cu(BTA)$_2$ complex that allows the nitrogen atoms to bond strongly with the surface copper atoms and the adatoms that hold the complex together. Then there is the stacking of successive Cu(BTA)$_2$ complexes in the $[001]$ direction, which is mediated through π-π van der Waals interactions. Indeed, the corresponding adsorption energy of $E_{ads} = -4.02$ eV per molecule, is the lowest for any of the Cu-BTA complexes we have optimised, including extended [Cu-BTA]$_n$ metal-organic chain oriented along $[1\bar{1}0]$. However, the adsorption energy of the c(4×2) system is still overall the lowest one, explaining why this phase forms at low molecular coverages, while the (6×1) is the structure observed by STM in the high coverage regime (*vide supra*).

In principle, the formation of Cu(BTA)$_2$ complexes can happen with the same geometry and distances for all three low-Miller index surfaces of copper since the $[1\bar{1}0]$ surface direction of Cu(110) has the same structural characteristics as the $[01\bar{1}]$ directions of Cu(100) and Cu(111) (see Fig. S12). However, the surface lattice parameters and the symmetry of Cu(111) are far less favourable for the formation of π-stacked chains of Cu(BTA)$_2$ complexes. In fact, for a commensurate molecular superstructure, distances of 2.56 Å, 5.11 Å or 4.41 Å would only be available on Cu(111) – corresponding to 1× or 2× periodicities along $[01\bar{1}]$ and to a 1× periodicity along the $[11\bar{2}]$, respectively (see Fig. S12). Indeed, although the same type of Cu(BTA)$_2$ metal-organic complexes have already been shown to play an important role in the interaction of BTAH with Cu(111)[17-19, 31], on that surface they are very close in energy to extended $[01\bar{1}]$-oriented [Cu-BTA]$_n$ metal-organic chains, which are also experimentally observed. Conversely, the Cu(100) surface would

allow for stacking at *d* = 3.61 Å along the $[010]$ and $[001]$ directions (see Fig. S12), but this would be a parallel-displaced π-stacking; moreover, the substrate and its ability to release any potential strain generated by the formation of $Cu(BTA)_2$ complexes might also play a role in the way these complexes organise onto the surface.

3.3. X-ray Photoelectron Spectroscopy

XPS measurements were carried out for a series of successive depositions, whereby the Cu(110) surface was exposed for increasing amounts of time to a BTAH pressure of 3×10^{-9} mbar. XP overview spectra were acquired together with higher resolution spectra in the Cu $2p_{3/2}$, N 1s and C 1s binding energy (BE) regions after each deposition step. Figure 7 shows the evolution of the relative intensities of the Cu $2p_{3/2}$, N 1s and C 1s peaks as a function of the cumulative exposure to BTAH. It should be noted that the measured values of the relative intensities of the N 1s and C 1s signals might be affected differently by inelastic photoelectron losses and/or by photoelectron diffraction effects (see later). Consequently, while these signals are proportional to the surface concentration of nitrogen and carbon, respectively, the proportionality factors might be different and could vary as a function of BTAH exposure. Moreover, the horizontal axis in Figure 7 should not be thought of as directly representing the total molecular coverage since the relation between BTAH exposure time and molecular coverage depends on the sticking coefficient of the molecules and this is likely to be coverage-dependent. Nevertheless, even when taking these effects into consideration, the data in Figure 7 indicate that the surface molecular coverage increases up to an exposure of about 400 s and then effectively saturates for further exposure. This is a clear demonstration of the self-limited nature of the upright BTA monolayer, in agreement with the STM observations.

The hollow data markers in Figure 7 were obtained after annealing the sample that had been exposed for 780 s to BTAH to 150 °C for 20 minutes; thus, based on what was observed in STM, this sample corresponds to the 3D nano-ridge phase. As a matter of fact, LEED measurements on this sample showed a pattern with characteristic stripes oriented at about +35° and −35° with respect to the $[001]$ direction (Fig. S9), thus compatible with the $[\bar{1}1\bar{2}]$ and $[\bar{1}12]$ orientations of the 3D nano-ridges as measured by STM. The other phases could however not be identified by LEED, as they were not stable under the electron beam. Nevertheless, an approximate assignment could be obtained by comparing the relative intensities of the C 1s and N 1s signals with the molecular densities of the phases determined by STM (see Table S1). By doing so, four different regimes could

be identified in the XPS experiments (see Fig. 7): (i) a low coverage regime, characterised by mostly flat BTA molecules mainly arranged in a c(4×2) superstructure; (ii) an intermediate coverage regime where c(4×2) regions coexist with regions of upright BTA molecules; (iii) a self-limiting, saturated high coverage regime where molecules are mostly upright in a local (3×1) arrangement; (iv) the 3D nano-ridge regime, obtained after annealing the high coverage phase to 150 °C. Based on this assignment, in the following we discuss the details of the fitting and the interpretation of the N 1s and C 1s XP spectra separately for the three main molecular phases of BTA on Cu(110).

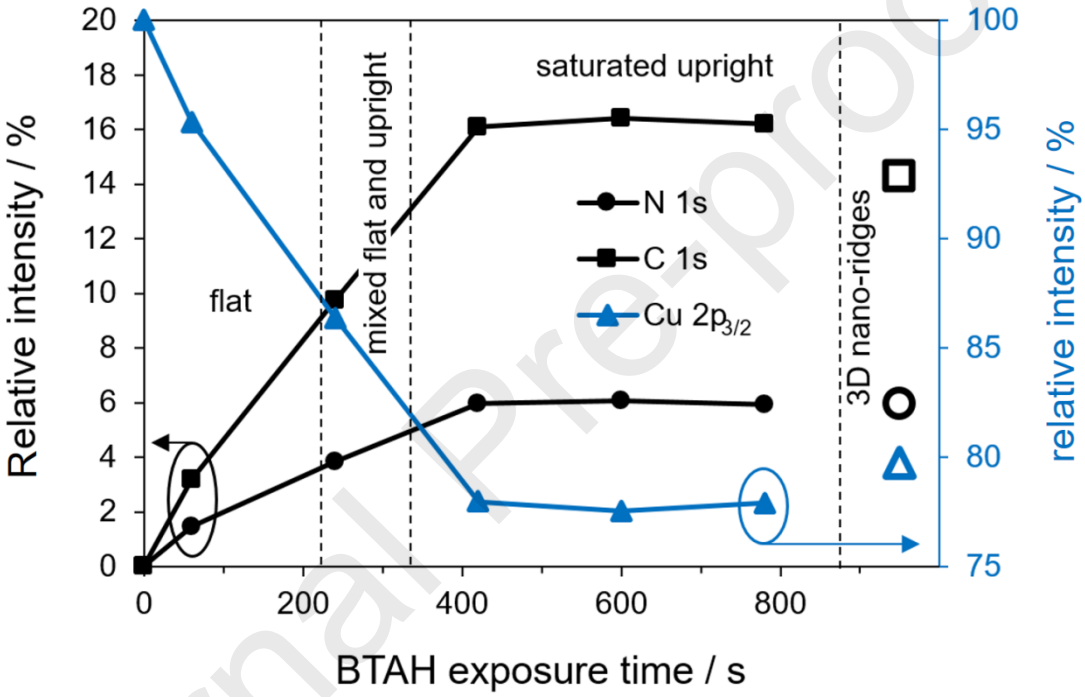

Fig. 7. Relative intensities of the Cu $2p_{3/2}$, N 1s and C 1s XPS signals as function of the BTAH exposure time for a pressure of 3×10^{-9} mbar. At any time, the sum of the three intensities adds to 1. Empty symbols refer to the 150 °C annealing of the saturated upright phase, corresponding to the 3D nano-ridges (see text). The vertical dashed lines separate the different observed phases; their position is only approximate.

3.3.1. Low coverage regime

The best fit to the N 1s spectra was obtained with two components (Fig. 8a). The peak at lower BE is assigned to the N-C environment (399.6 eV, orange), while the peak at higher BE (400.4 eV, blue) is assigned to the N-N environment, in close agreement with previous literature[18]. The absence of a third peak at even higher BE, typically assigned to the H-N-C environment[51], confirms that

molecules are in the fully deprotonated state. The ratio between the integrated intensities of the two peaks is ~1.5 which is close to the expected ratio of 2. The departure from the ideal ratio might be due to slight differences in the N-Cu local binding environments of the three nitrogen atoms, which has been shown to cause chemical shifts of up to 0.8 eV[18] and could thus rebalance the relative intensities of the N-C and N-N species. The C 1s spectrum is also best fit with two components (Fig. 8b), a lower BE peak (284.9 eV, red) assigned to the C-C environment and a higher BE peak (285.6 eV, purple) assigned to the C-N environment[51]. The ratio between the integrated intensities in this case is ~1.3, which is quite far from the expected ratio of 2 between C-C and C-N environments. We do not have a clear explanation for this observation, which was however consistently confirmed in numerous repeat experiments. We speculate that it might be due to inelastic photoelectron losses and/or to photoelectron diffraction effects.

3.3.2. High coverage regime

In this coverage regime, the N 1s spectrum is best fit with three components (Fig. 8c). The two peaks at lower BE (399.7 eV, orange, and 400.7 eV, blue) have an almost identical position as those measured for the lower coverage phase and are thus similarly assigned to the N-C and the N-N environments, respectively. The presence of a third peak at higher BE (401.7 eV, green) is assigned to the H-N-C environment of protonated (and possibly hydrogen-bonded) BTAH molecules adsorbed atop of the first upright BTA layer (most likely, the second-layer physisorbed mobile molecules identified in STM). Based on this assignment, it is possible to evaluate the relative contribution of the BTAH and the BTA molecules to the N 1s spectrum, which results in a percentage of second-layer protonated molecules around 20-30% (see Figs. S7 and S8). This is in good agreement with what we observed in STM (*vide supra*) and with previous data reported in the literature for the BTAH/Cu(111) system[18], the BTAH/Cu/Au(111) system[51] and for a BTAH film on copper prepared from solution[52].

The C 1s spectrum for the high coverage regime is best fitted with three components (Fig. 8d). The two peaks at lower BE (284.7 eV, red, and 285.3 eV, purple) are almost rigidly shifted by 0.3-0.4 eV with respect to the two corresponding C 1s components measured at low coverage (Fig. 8b) and are thus assigned to the C-C and C-N environments, respectively. The shift to lower binding energies was also observed in a similar system[51] and might be the result of changes in the surface dipole layer generated by the BTA molecules when they are oriented almost parallel to the surface (low

coverage) or almost perpendicular to it (high coverage). The origin of the third peak at higher BE (286.1 eV, cyan) is not clear although it must be related to the loosely bound second-layer molecules because it disappears after annealing (see Fig. 8f). While the carbon atoms should not be directly affected by the protonation of the triazole group, one could speculate that physisorbed BTAH molecules might undergo C-H···N hydrogen bonds and that this could create a slightly different chemical environment for the C 1s core electrons resulting in a higher BE component. Interestingly, a very similar high BE shoulder was observed also for BTAH deposited on Cu/Au(111)[51].

3.3.3. 3D nano-ridges

The N 1s spectrum measured after having annealed the high coverage phase to 150 °C lacks the higher binding energy shoulder, indicating that the second layer species have desorbed. The best fit is obtained with only two components (Fig. 8e) centred at 399.6 eV (orange) and 400.5 eV (blue), respectively; these are just slightly shifted with respect to the corresponding ones in the pre-annealed phase and are therefore similarly assigned to the N-C and the N-N environments, respectively. The relative intensity of these peaks is in the expected ratio of 2:1. After annealing, the higher BE component in the C 1s spectrum disappears (Fig. 8f) and the best fit is obtained with two components (284.8 eV, red, and 285.4 eV, purple), virtually unchanged with respect to the pre-annealing phase and thus assigned to the same C-C and C-N environments, respectively. Similarly to the case before annealing, also here the relative intensity of these two components if far from the expected 2:1 ratio.

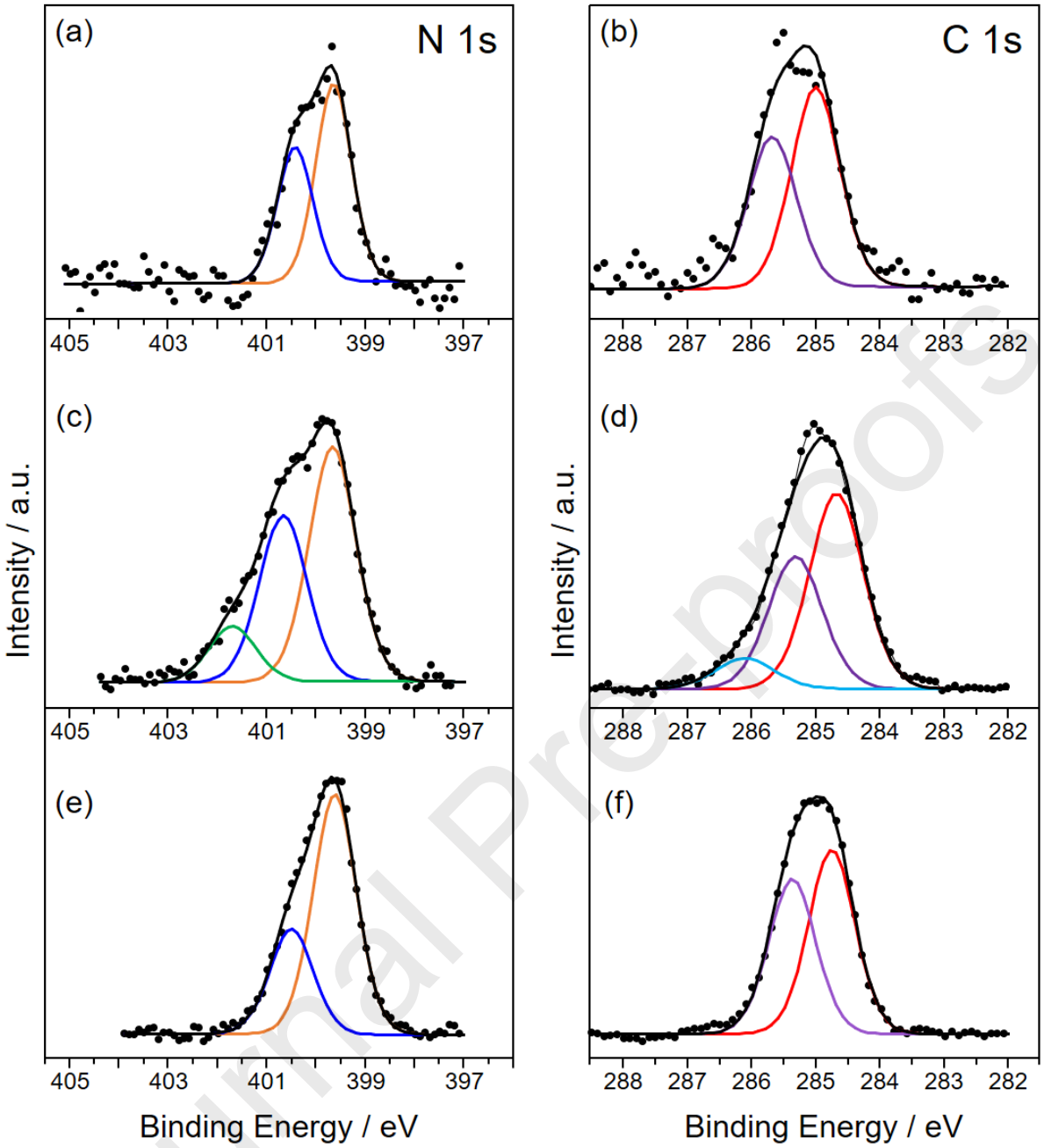

Fig. 8. XP spectra in the N 1s (left column) and C 1s (right column) BE regions for different molecular phases formed by exposing the Cu(110) surface to a BTAH pressure of 3×10^{-9} mbar and increasing amounts of time. (a) N 1s spectrum after 60 s of BTAH exposure, resulting in low coverage phases characterised by mostly flat BTA molecules; (b) corresponding C 1s spectrum. (c) N 1s spectrum after 780 s of BTAH exposure, resulting in the high coverage phase characterised by mostly upright BTA molecules; (d) corresponding C 1s spectrum. (e) N 1s spectrum of the sample in (c) after 780 s annealing to 150 °C resulting in the formation of 3D nano-ridges; (f) corresponding C 1s spectrum. The data points are shown by black circles, the best fit curve by a black line, while coloured lines indicate the different fit components.

3.4. High Resolution Electron Energy Loss Spectroscopy

Vibrational spectra following deposition of BTAH on Cu(110) and annealing are shown in Fig. 9. Energy losses observed experimentally, and their assignments, are summarised for ease of comparison in Table 1.

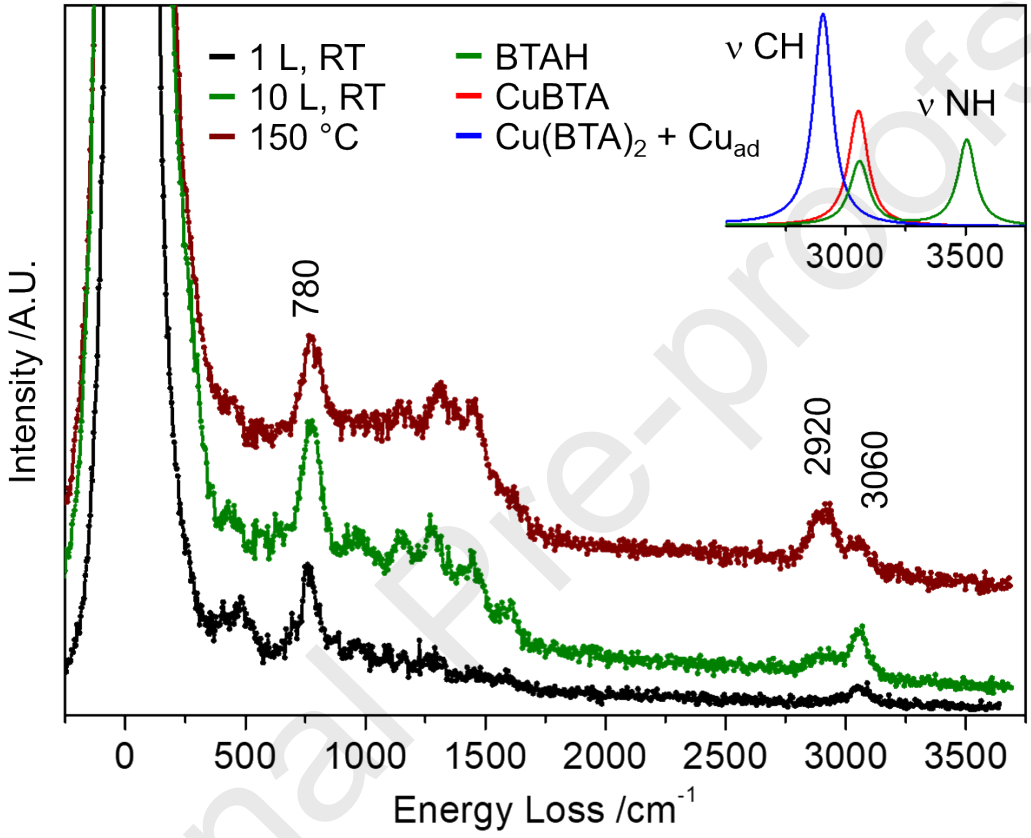

Fig. 9. HREEL spectra following deposition of BTAH on Cu(110) at room temperature and annealing to 150 °C. Spectra are offset vertically for clarity. BTAH exposures are indicated in langmuir (L). In the inset: calculated ν NH and ν CH vibrational region for BTAH and two Cu_xBTA_y species evaluated via DFT methods (see SM).

Table1. Observed energy losses /cm^{-1} and assignments. BTAH exposures are indicated in langmuir (L).

Mode	1 L, RT	10 L, RT	150 °C
ν CH ($Cu_{(i)}BTA$)	3065	3065	3055
ν CH ($CuBTA_2$)		2910	2905
ν CC + ν CN		1605	1610
δ NH (H-bonded)	1585		
ν_{asym} C_6H_4	1470	1460	1455
γ CH + breathing			1315
ν NNN (N… Cu(I))	1285	1290	
ν NNN + ν CH	1155	1150	1160
γ NH (H-bonded) + w CH	960	960	
γ CH	760	780	765
C_6H_4 ring breathing		650	
γ C_6H_4	470	540	
γ C_6H_4		430	425

ν stretch, γ out of pane bend, δ in plane bend, τ torsion, w wag

The HREEL spectrum recorded for the low coverage regime at room temperature, 1 L (130 s × 1×10^{-8} mbar, black trace), shows energy loss modes at 470 cm^{-1} (with a possible shoulder at 430 cm^{-1}), due to out of plane deformations of the benzene ring (γ C_6H_4); at 760 cm^{-1}, corresponding to a C-H out of plane mode of the benzene ring, γ CH; and at 3065 cm^{-1}, corresponding to C-H stretches of the benzene ring, ν CH. Typically, a γ C_6H_4 deformation is observed for flat lying BTAH[53], and would be expected also for BTA. However, the spectral fingerprint of a flat lying molecule usually also shows a high γ CH :ν CH ratio[53], the ν CH being largely forbidden because it is dipole inactive, which is not the case in the present spectrum. The energy loss at *ca.* 960 cm^{-1} could be assigned to the γ NH (coupled with a CH wag) and that at *ca.* 1585 cm^{-1} to δ NH, both for hydrogen bonded BTAH[53]. These, along with the presence of additional vibrations in the region 800 – 1600 cm^{-1}, can indicate the coexistence of species adsorbed with their molecular plane at a small angle with respect to the surface[51]. In fact, the modes at *ca*. 1285 cm^{-1} and 1155 cm^{-1} are assigned to stretches of the triazole group in an N…Cu(I) environment[54] and coupled with ν CH respectively; these may indicate that formation of some Cu_xBTA_y species has occurred, and are expected to be dipole active only for inclined/upright adsorption[17]. The energy loss at *ca.* 1470 cm^{-1} is assigned to CH asymmetric stretches. These HREELS observations are compatible with the presence of the c(4×2) phase, where the molecules have their molecular planes not completely flat, as previously discussed

in the STM (because of steric reasons, see model in Fig. 2d) and in the DFT (see Fig. 5) sections. However, as determined by taking into account the XPS measurements at low coverage, in the c(4×2) phase the molecules are fully deprotonated and thus the signature of the N-H moiety indicates that the coverage is already in the "mixed flat and upright" regime, see Fig. S8. This latter phase is characterised by flat-lying BTAH molecules physisorbed on top of the c(4×2) phase; hence the dipole generated by their γ CH vibration is dampened and the mode has a low intensity, while those generated by ν CH and ν NH are dipole inactive.

Several differences in the energy loss spectrum are seen at increased coverage (total of 10 L, room temperature, olive trace). The peak at 470 cm^{-1} is replaced by one at 430 cm^{-1}; a peak at 650 cm^{-1} is assigned to a benzene ring breathing motion; the γ CH shifts to 780 cm^{-1} and broadens slightly. The broadening is the result of the summation of γ CH vibrations generated by additional tilted species, with a weak contribution from species orientated almost upright, as γ CH is dipole inactive for a fully upright geometry. The 800 – 1600 cm^{-1} region is more resolved. In the ν CH region, a peak appears at *ca.* 2910 cm^{-1}. Calculated spectra shown in Fig. S11 help in rationalising the broadening of the γ CH signal and in assigning the peaks observed in the ν CH region. The γ CH of both BTAH and CuBTA are calculated at *ca*. 790 cm^{-1}, whereas that of $Cu(BTA)_2$ is calculated at about 860 cm^{-1}. A downshift of the vibration for both species could be due to a packing effect, tentatively π-π stacking. Additionally, as shown in the inset in Fig. 9, both BTAH and CuBTA have a calculated CH stretch at 3055 cm^{-1}, whereas that of $Cu(BTA)_2$ – in this case including some additional copper adatoms, see Figs. S10 and S11 – falls at 2905 cm^{-1}. A downshift for an aromatic ν CH was recently reported upon metal complexation of di-pyridyl-tetrazine on Ag(111)[55], and ascribed to the presence of the metal which could render the aryl C-H more aliphatic. The HREELS fingerprint is very similar to that recorded for high coverage BTAH on Cu(111), which was determined to consist mainly of $Cu(BTA)_2$ species, with some minor contribution due to CuBTA, all adsorbed upright[17]. In the present case, however, based on the relative intensity of the corresponding ν CH stretches, the surface concentration of adsorbed CuBTA is thought to be higher than that of $Cu(BTA)_2$. These results are fully compatible with the STM data in Fig. 3 showing that, at high coverage, the mostly flat lying species are displaced such that adsorbed molecules adopt an upright geometry in a local (3×1) or (6×1) superstructure stabilised by π-π interactions (see also DFT results). In particular, it can be proposed that the CuBTA species could correspond to the single features constituting the (3×1)

phase of Fig. 3, whereas the $Cu(BTA)_2$ species could correspond to the local pairing of molecules highlighted in Fig. S5a.

On annealing to 150 °C (brown trace), a general decrease of the intensity is seen, in particular for the w CH and (ν CC + ν CN) signals. In the ν CH region, the peak associated to $Cu(BTA)_2$ becomes more intense than that associated with CuBTA. Upon annealing to this temperature, STM images (Fig. 4) show the formation of 3D nano-ridges essentially created by a strong interaction of BTA with copper atoms, inducing a high degree of surface reconstruction and a significant increase in short- and long-range order. STM images also show features attributed to single BTA molecules decorating the step-edges of the mini-terraces constituting the flanks of the 3D nano-ridges. In agreement to this description, the HREEL spectrum indicates that both $Cu(BTA)_2$ and CuBTA species are present.

4. Conclusion

A combined experimental (STM, XPS, HREELS) and theoretical (DFT) investigation of the interaction of benzotriazole molecules with a Cu(110) single crystal has been performed. Different supramolecular structures have been observed depending on the BTAH exposure, with XPS showing that the molecules directly in contact with the copper substrate are always in the deprotonated BTA form. At low coverages, the surface is dominated by BTA molecules adsorbed almost flat and organised in a c(4×2) supramolecular structure. Upon increasing the molecular coverage, a gradual transformation towards a higher density phase occurs, where BTA molecules adsorb in an almost upright configuration until a self-limiting monolayer is formed. This phase is characterised by the inclusion of copper adatoms that bind to BTA molecules in Cu(BTA) and $Cu(BTA)_2$ metal-organic complexes. Moreover, π-π stacking between the aromatic rings of BTA molecules causes an alignment of the complexes along the $[001]$ substrate direction forming wavy rows with a local (3×1) and (6×1) periodicity. Annealing to 150°C results in a major transformation that involves a substantial in-plane and out-of-plane reconstruction of the Cu(110) substrate with the development of 3D nano-ridges decorated by long-range ordered rows of Cu(BTA) and $Cu(BTA)_2$ complexes.

Although several characteristics of the observed molecular phases are closely dependent on the specific energetics and structure of the Cu(110) surface – e.g. the molecular lateral packing that is clearly templated by the substrate and the 3D nano-ridges reconstruction that is facilitated by the open nature of the Cu(110) surface and by its strong in-plane anisotropy – a few general features

appear to be common to the BTAH/Cu(111) system[16, 17]. In particular, this is true for the deprotonation of molecules in direct contact with the copper substrate, the transition from a mostly flat to a mostly upright adsorption configuration with increasing molecular coverage and, crucially, the formation of strongly bound $Cu(BTA)_2$ metal-organic complexes. The presented result are a further important step in the characterisation of the interaction of BTAH with copper surfaces and are expected to be of relevance for the development of a molecular-scale understanding of the action mechanism of this prototypical molecular corrosion inhibitor for copper.

Acknowledgements

O. De Luca is acknowledged for useful discussion on the interpretation of XPS data. M.T. gratefully acknowledges financial support from Lubrizol Limited and, together with J.E., thank the Engineering and Physical Sciences Research Council (EPSRC) grant EP/L015307/1 for the Molecular Analytical Science Centre for Doctoral Training (MAS-CDT). F.G. acknowledges the participation of D. W. Tee in collecting part of the HREELS data and the EaStCHEM Research Computing facility for providing computational resources for the gas phase modelling of HREELS data. C.G acknowledges the Euler cluster managed by the HPC team at ETH Zurich for computational resources and is grateful for computational support from the UK national high performance computing service, ARCHER, for which access was obtained via the UKCP consortium and funded by EPSRC grant EP/P022561/1.

Data statement

All data needed to evaluate the conclusions in the paper are present in the paper and/or the Electronic Supplementary Material. Additional data related to this paper may be requested from the authors.

Author statement

MT performed and analysed the STM measurements, analysed the XPS data and wrote a first draft of the manuscript. MW performed the XPS measurements and participated in their analysis. FG helped in devising the experimental plan, performed and analysed the HREELS measurements and wrote the corresponding part of the paper. CG performed and analysed the DFT calculations and

wrote the corresponding part of the paper. JE performed preliminary STM measurements. OA participated in the analysis of the XPS data. GH and PK proposed the scientific problem, contributed to the conception of the project and discussed the STM data. NVR and CJB discussed the analysis of HREELS data. AM advised and discussed the DFT work. GC conceived and coordinated the research project and wrote most of the paper. All authors participated in discussing the data and editing the manuscript.

Declaration of competing interest

The authors declare that they have no known competing financial interests or personal relationships that could have appeared to influence the work reported in this paper.

Appendix A. Supplementary material

Supplementary data to this article can be found online at https://doi. org/xxxxxx

References

[1] M. Finšgar, I. Milošev, Inhibition of copper corrosion by 1, 2, 3-benzotriazole: a review, Corr. Sci., 52 (2010) 2737-2749.
[2] International Measures of Prevention, Application and Economics of Corrosion Technologies Study, NACE International IMPACT, http://impact.nace.org/economic-impact.aspx, 2016 (accessed 12 July 2021).
[3] J.R. Davis, Copper and copper alloys, ASM international, Materials Park (Ohio), 2001.
[4] A.M. El-Sherik, Trends in Oil and Gas Corrosion Research and Technologies, Woodhead Publishing, Cambridge, 2017.
[5] C. Gattinoni, A. Michaelides, Atomistic details of oxide surfaces and surface oxidation: the example of copper and its oxides, Surf. Sci. Rep., 70 (2015) 424-447.
[6] A. Fateh, M. Aliofkhazraei , A.R. Rezvanian, Review of corrosive environments for copper and its corrosion inhibitors, Arab. J. Chem., 13 (2017) 1-64.

[7] Y.I. Kuznetsov, Triazoles as a class of multifunctional corrosion inhibitors. A review. Part I. 1, 2, 3-Benzotriazole and its derivatives. Copper, zinc and their alloys, Int. J. Corros., 7 (2018) 271-307.
[8] Procter and Gamble Ltd, Compositions for Inhibiting Metal Tarnish, British Patent, 1947.
[9] C.D.A. Inc., Benzotriazole: An effective corrosion inhibitor for copper alloys, Copper Development Association, https://www.copper.org/publications/pub_list/pdf/a1349.pdf , 2021 (accessed 12 Jul 2021).
[10] A. Kokalj, S. Peljhan, Density functional theory study of ATA, BTAH, and BTAOH as copper corrosion inhibitors: adsorption onto Cu (111) from gas phase, Langmuir, 26 (2010) 14582-14593.
[11] A. Kokalj, S. Peljhan, M. Finsgar, I. Milosev, What determines the inhibition effectiveness of ATA, BTAH, and BTAOH corrosion inhibitors on copper?, J. Am. Chem. Soc., 132 (2010) 16657-16668.
[12] S. Peljhan, A. Kokalj, DFT study of gas-phase adsorption of benzotriazole on Cu (111), Cu (100), Cu (110), and low coordinated defects thereon, Phys. Chem. Chem. Phys., 13 (2011) 20408-20417.
[13] I. Dugdale, J. Cotton, An electrochemical investigation on the prevention of staining of copper by benzotriazole, Corr. Sci., 3 (1963) 69-74.
[14] K. Mansikkamäki, C. Johans, K. Kontturi, The effect of oxygen on the inhibition of copper corrosion with benzotriazole, J. Electrochem. Soc., 153 (2005) B22.
[15] J. Walsh, H. Dhariwal, A. Gutierrez-Sosa, P. Finetti, C. Muryn, N. Brookes, R. Oldman, G. Thornton, Probing molecular orientation in corrosion inhibition via a NEXAFS study of benzotriazole and related molecules on Cu (100), Surf. Sci., 415 (1998) 423-432.
[16] F. Grillo, D.W. Tee, S.M. Francis, H. Früchtl, N.V. Richardson, Initial stages of benzotriazole adsorption on the Cu (111) surface, Nanoscale, 5 (2013) 5269-5273.
[17] F. Grillo, D.W. Tee, S.M. Francis, H.A. Früchtl, N.V. Richardson, Passivation of copper: benzotriazole films on Cu (111), J. Phys. Chem. C, 118 (2014) 8667-8675.
[18] C. Gattinoni, P. Tsaousis, C. Euaruksakul, R. Price, D.A. Duncan, T. Pascal, D. Prendergast, G. Held, A. Michaelides, Adsorption behavior of organic molecules: a study of benzotriazole on Cu (111) with spectroscopic and theoretical methods, Langmuir, 35 (2019) 882-893.
[19] X. Chen, H. Häkkinen, Divide and protect: passivating Cu (111) by Cu-(benzotriazole) 2, J. Phys. Chem. C, 116 (2012) 22346-22349.
[20] K. Cho, J. Kishimoto, T. Hashizume, T. Sakurai, An Observation of Benzotriazole (BTA) Adsorption on Cu (110) by the Ultra High Vacuum (UHV)-Scanning Tunneling Microscope (STM) and Low Energy Electron Difiraction (LEED), Jpn. J. Appl. Phys., 33 (1994) L125.
[21] I. Horcas, R. Fernández, J. Gomez-Rodriguez, J. Colchero, J. Gómez-Herrero, A. Baro, WSXM: a software for scanning probe microscopy and a tool for nanotechnology, Rev. Sci. Instrum., 78 (2007) 013705.
[22] CasaXPS software version 2.3.22, in, Casa Software Ltd, Teignmouth, UK.
[23] J. Frisch, W. Trucks, B. Schlegel, Gaussian 09, Revision D. 01, Gauss, 2013.
[24] T. Kasahara, H. Shinohara, Y. Oshima, K. Kadokura, Y. Uriu, C. Ohe, K. Itoh, Infrared reflection absorption spectroscopic studies on the adsorption structures of dimethyl sulfide and methyl ethyl sulfide on Ag (1 1 0) and Cu (1 1 0), Surf. Sci., 558 (2004) 65-79.
[25] G. Kresse, J. Furthmüller, Efficiency of ab-initio total energy calculations for metals and semiconductors using a plane-wave basis set, Comput. Mater. Sci., 6 (1996) 15-50.

[26] G. Kresse, J. Furthmüller, Efficient iterative schemes for ab initio total-energy calculations using a plane-wave basis set, Phys. Rev. B, 54 (1996) 11169.
[27] G. Kresse, J. Hafner, Ab initio molecular dynamics for liquid metals, Phys. Rev. B, 47 (1993) 558.
[28] J. Klimeš, D.R. Bowler, A. Michaelides, Van der Waals density functionals applied to solids, Phys. Rev. B, 83 (2011) 195131.
[29] G. Kresse, D. Joubert, From ultrasoft pseudopotentials to the projector augmented-wave method, Phys. Rev. B, 59 (1999) 1758.
[30] N. Simon, E. Drexler, R. Reed, Properties of copper and copper alloys at cryogenic temperatures. Final report, National Inst. of Standards and Technology (MSEL), Boulder, Washington, 1992.
[31] C. Gattinoni, A. Michaelides, Understanding corrosion inhibition with van der Waals DFT methods: the case of benzotriazole, Faraday Discuss., 180 (2015) 439-458.
[32] S. Peljhan, J. Koller, A. Kokalj, The effect of surface geometry of copper on adsorption of benzotriazole and Cl. Part I, J. Phys. Chem. C, 118 (2014) 933-943.
[33] Y. Wang, S. Fabris, T.W. White, F. Pagliuca, P. Moras, M. Papagno, D. Topwal, P. Sheverdyaeva, C. Carbone, M. Lingenfelder, T. Classen, K. Kern, G. Costantini, Varying molecular interactions by coverage in supramolecular surface chemistry, Chem. Commun., 48 (2012) 534-536.
[34] T. Classen, M. Lingenfelder, Y. Wang, R. Chopra, C. Virojanadara, U. Starke, G. Costantini, G. Fratesi, S. Fabris, S. De Gironcoli, Hydrogen and coordination bonding supramolecular structures of trimesic acid on Cu (110), J. Phys. Chem. A, 111 (2007) 12589-12603.
[35] L. Dong, Z.A. Gao, N. Lin, Self-assembly of metal–organic coordination structures on surfaces, Prog. Surf. Sci., 91 (2016) 101-135.
[36] C. Perry, S. Haq, B. Frederick, N. Richardson, Face specificity and the role of metal adatoms in molecular reorientation at surfaces, Surf. Sci., 409 (1998) 512-520.
[37] A. Della Pia, M. Riello, J. Lawrence, D. Stassen, T.S. Jones, D. Bonifazi, A. De Vita, G. Costantini, Two-Dimensional Ketone-Driven Metal–Organic Coordination on Cu (111), Chemistry, 22 (2016) 8105.
[38] A.C. Papageorgiou, J. Li, S.C. Oh, B. Zhang, Ö. Sağlam, Y. Guo, J. Reichert, A.B. Marco, D. Cortizo-Lacalle, A. Mateo-Alonso, Tuning the ease of formation of on-surface metal-adatom coordination polymers featuring diketones, Nanoscale, 10 (2018) 9561-9568.
[39] J. Björk, M. Matena, M.S. Dyer, M. Enache, J. Lobo-Checa, L.H. Gade, T.A. Jung, M. Stöhr, M. Persson, STM fingerprint of molecule–adatom interactions in a self-assembled metal–organic surface coordination network on Cu (111), Phys. Chem. Chem. Phys., 12 (2010) 8815-8821.
[40] C. Wäckerlin, C. Iacovita, D. Chylarecka, P. Fesser, T.A. Jung, N. Ballav, Assembly of 2D ionic layers by reaction of alkali halides with the organic electrophile 7, 7, 8, 8-tetracyano-p-quinodimethane (TCNQ), Chem. Commun., 47 (2011) 9146-9148.
[41] M.N. Faraggi, N. Jiang, N. Gonzalez-Lakunza, A. Langner, S. Stepanow, K. Kern, A. Arnau, Bonding and charge transfer in metal–organic coordination networks on Au (111) with strong acceptor molecules, J. Phys. Chem. C, 116 (2012) 24558-24565.
[42] A. Della Pia, M. Riello, D. Stassen, T. Jones, D. Bonifazi, A. De Vita, G. Costantini, Two-dimensional core–shell donor–acceptor assemblies at metal–organic interfaces promoted by surface-mediated charge transfer, Nanoscale, 8 (2016) 19004-19013.
[43] J. Rodríguez-Fernández, K. Lauwaet, M.Á. Herranz, N. Martín, J.M. Gallego, R. Miranda, R. Otero, Temperature-controlled metal/ligand stoichiometric ratio in Ag-TCNE coordination networks, J. Chem. Phys., 142 (2015) 101930.
[44] T.W. White, N. Martsinovich, A. Troisi, G. Costantini, Quantifying the “Subtle Interplay” between Intermolecular and Molecule–Substrate Interactions in Molecular Assembly on Surfaces, J. Phys. Chem. C, 122 (2018) 17954-17962.
[45] E. Goiri, J. García-Lastra, M. Corso, Z. Adb El-Fattah, J.E. Ortega, D. de Oteyza, Understanding periodic dislocations in 2D supramolecular crystals: The PFP/Ag (111) interface, J. Phys. Chem. Lett., 3 (2012) 848-852.
[46] K. Cho, J. Kishimoto, T. Hashizume, H. Pickering, T. Sakurai, Adsorption and film growth of BTA on clean and oxygen adsorbed Cu (110) surfaces, Appl. Surf. Sci., 87 (1995) 380-385.

[47] Y. Park, H. Noh, Y. Kuk, K. Cho, T. Sakurai, Thickness dependent ultraviolet photoemission spectroscopy and scanning tunneling microscopy study of BTA molecular layers on Cu (110), J. Korean Phys. Soc., 29 (1996) 745-749.
[48] M.O. Sinnokrot, C.D. Sherrill, Substituent effects in π− π interactions: sandwich and T-shaped configurations, J. Am. Chem. Soc., 126 (2004) 7690-7697.
[49] F. Cunha, N. Tao, Surface charge induced order-disorder transition in an organic monolayer, Phys. Rev. Lett., 75 (1995) 2376.
[50] C. Janiak, A critical account on π–π stacking in metal complexes with aromatic nitrogen-containing ligands, J. Chem. Soc., Dalton trans., (2000) 3885-3896.
[51] F. Grillo, D. Batchelor, C.R. Larrea, S.M. Francis, P. Lacovig, N.V. Richardson, On-surface condensation of low-dimensional benzotriazole–copper assemblies, Nanoscale, 11 (2019) 13017-13031.
[52] G. Xue, J. Ding, Chemisorption of a compact polymeric coating on copper surfaces from a benzotriazole solution, Appl. Surf. Sci., 40 (1990) 327-332.
[53] F. Grillo, J.G. Torres, M.J. Treanor, C.R. Larrea, J.P. Goetze, P. Lacovig, H. Früchtl, R. Schaub, N.V. Richardson, Two-dimensional self-assembly of benzotriazole on an inert substrate, Nanoscale, 8 (2016) 9167-9177.
[54] K. Salorinne, X. Chen, R.W. Troff, M. Nissinen, H. Häkkinen, One-pot synthesis and characterization of subnanometre-size benzotriazolate protected copper clusters, Nanoscale, 4 (2012) 4095-4098.
[55] C.G. Williams, M. Wang, D. Skomski, C.D. Tempas, L.L. Kesmodel, S.L. Tait, Metal–Ligand Complexation through Redox Assembly at Surfaces Characterized by Vibrational Spectroscopy, J. Phys. Chem. C, 121 (2017) 13183-13190.